Deep-Sea Research II 118 (2015) 7–17

Contents lists available at ScienceDirect

Deep-Sea Research II

journal homepage: www.elsevier.com/locate/dsr2

Physical and morphological properties of sea ice in the Chukchi and Beaufort Seas during the 2010 and 2011 NASA ICESCAPE missions

Chris Polashenski [a,b,*], Donald K. Perovich [a,b], Karen E. Frey [c], Lee W. Cooper [d], Christie I. Logvinova [c], Ruzica Dadic [f], Bonnie Light [g], Holly P. Kelly [d,e], Luke D. Trusel [c], Melinda Webster [g]

[a] *ERDC-CRREL, USA*
[b] *Dartmouth College, USA*
[c] *Clark University, USA*
[d] *University of Maryland Center for Environmental Science, USA*
[e] *424 Russfield Dr Knoxville, TN 37922, USA*
[f] *University of Wellington, New Zealand*
[g] *University of Washington, USA*

ARTICLE INFO

Available online 14 April 2015

Keywords:
Sea ice properties
In situ measurements
Arctic zone

ABSTRACT

Physical and morphological properties of sea ice in the Chukchi and western Beaufort seas were measured during the 2010 and 2011 June – July ICESCAPE (Impacts of Climate on the Eco-Systems and Chemistry of the Arctic Pacific Environment) missions aboard the *USCGC Healy*. Observations of ice conditions, including ice thicknesses, types, and concentrations of primary, secondary, and tertiary categories were reported at 2-h intervals while the ship was in transit using the Antarctic Sea ice Processes and Climate (ASPeCt) protocol. On-ice surveys of ice thickness, melt-pond depth, and ice properties (including profiles of internal temperature, salinity, and isotopic composition) were conducted at 21 total ice stations (12 in 2010 and 9 in 2011). Comparison to historical ship-based observations confirms a multi-decadal transition from a multiyear to thinner, first year -dominated seasonal sea-ice pack in the region, with much earlier ice retreat than in past decades. The ice encountered was predominantly (> 98%) first year, with un-deformed ice thicknesses ranging from 0.73 to 1.2 m. Pond coverage was extensive, averaging 29% in 2010 and 19% in 2011, resulting in considerable light absorption in the ice and transmission of light to the ocean. Enhanced melting near the ice edge is consistent with transport of Pacific-origin heat and/or ice-albedo feedbacks. Sediment entrainment was visible in 7.5% and 10.9% of the ice in 2010 and 2011, respectively. Overall, the results indicate a regime shift in the characteristics of the ice cover has occurred in the region over recent decades, with substantive implications for thermodynamic forcing, light availability in the upper ocean, and biological and biogeochemical processes in the ice and water column beneath. The results presented have applications for the interpretation of optical and biological measurements in the Chukchi Sea and serve as record of ice conditions for assessing long-term change.

Published by Elsevier Ltd.

1. Introduction

Seasonal sea ice cover in the Arctic has undergone a dramatic decline in recent years, including a decrease in summer ice extent (Comiso, 2012; Cavalieri and Parkinson, 2012; Jeffries et al., 2013) and thickness (Giles et al., 2008; Kwok and Rothrock, 2009; Haas et al., 2010; Laxon et al., 2013), a shift from perennial ice to younger, more vulnerable seasonal ice (Maslanik et al., 2011), and a change in the seasonality of melt and freezeup (Markus et al., 2009). The thick, perennially persistent ice cover that nearly filled the Arctic Basin in the 1980s is being replaced by thinner seasonal ice, particularly around the periphery of the basin. Passive microwave remote sensing data have shown that the decline in seasonal ice extent is particularly pronounced in the Chukchi and Beaufort seas, where increased summer ice retreat has resulted in large areas of open water and a transition to younger ice cover (Comiso, 2012).

Changes in ice-albedo energy feedbacks, light availability, and ocean – atmosphere heat and mass exchanges driven by ice cover change have significant implications for the biological communities of the Chukchi and Beaufort seas. Increased exposure of low-albedo open water during the sunlit months, earlier onset of melt, changes in melt

* Corresponding author.

http://dx.doi.org/10.1016/j.dsr2.2015.04.006
0967-0645/Published by Elsevier Ltd.

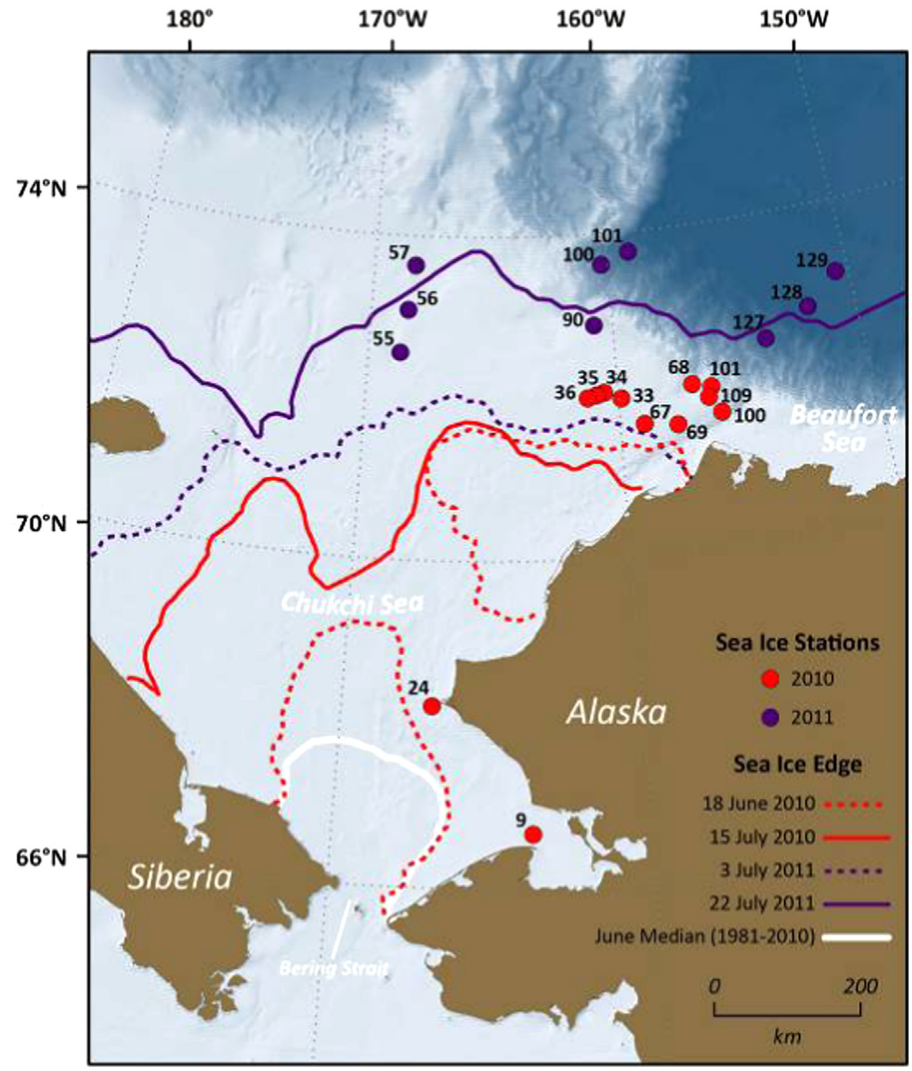

Fig. 1. Ice stations in 2010 (red) and 2011 (purple). The map includes the general area of the cruises. Also plotted are the positions of the ice edge at the beginning and end of the ice station portion of the cruises. (For interpretation of the references to color in this figure legend, the reader is referred to the web version of this article.)

pond coverage atop the ice, and changes of the ice albedo each may be playing a role in allowing greater transmission of solar radiation into the upper ocean (Nghiem et al., 2007; Perovich et al., 2008; Perovich et al., 2011; Perovich and Polashenski, 2012). The presence of large under-ice phytoplankton blooms observed during the NASA ICESCAPE mission in 2011 (Arrigo, et al., 2012) shows that penetration of light through the ice is sufficient to support enormous amounts of primary productivity, even beneath compact ice. The light availability in an ice covered ocean is related to the character and morphology of the ice cover, particularly its thickness, snow cover, and melt pond coverage. Here we present detailed in situ observations of ice morphology (e.g. thickness, type, sediment content) and physical properties (e.g. salinity, isotopic composition, crystallogrphy) collected during the ICESCAPE mission, capturing the conditions prevailing in 2010–2011 as a benchmark for future change and comparing them to past conditions in the Chukchi – Beaufort region.

2. Methods

2.1. Cruise track

The 2010 and 2011 ICESCAPE cruise tracks of the USCG *Healy* (Fig. 1) were designed to sample several important components of the Chukchi-Beaufort physical and biological systems including dominant ocean currents, mixing events, phytoplankton productivity hotspots, and varied ice conditions. Ice was encountered in the Chukchi Sea from June 18 to July 15, 2010 and July 3 to July 22, 2011 (see ice extent in Fig. 1, plotted for beginning and end dates of ice operations). Depending on ice conditions, ship speeds ranged from a few knots to little forward progress, with multiple backing and ramming maneuvers required. The timing of the cruise both years was set to start 2–4 weeks into the melt season and extend into the height of melt. During the two cruises, two categories of measurements were collected. In-transit observations, which were collected visually from the ship's bridge every 2 h while the ship was moving, and on-ice observations, which were collected at 21 ice stations.

2.2. In-transit observations

Ship-based sea ice observing methods incorporate some bias, owing to a preference of the ships' navigators for avoiding particularly thick ice, and the influence of this bias is challenging to quantify (Fig. 2). While ice concentration and conditions did influence the route choice during the ICESCAPE missions, much of the route was chosen to conduct straight line oceanographic transects, and therefore represents pseudo-random sampling of

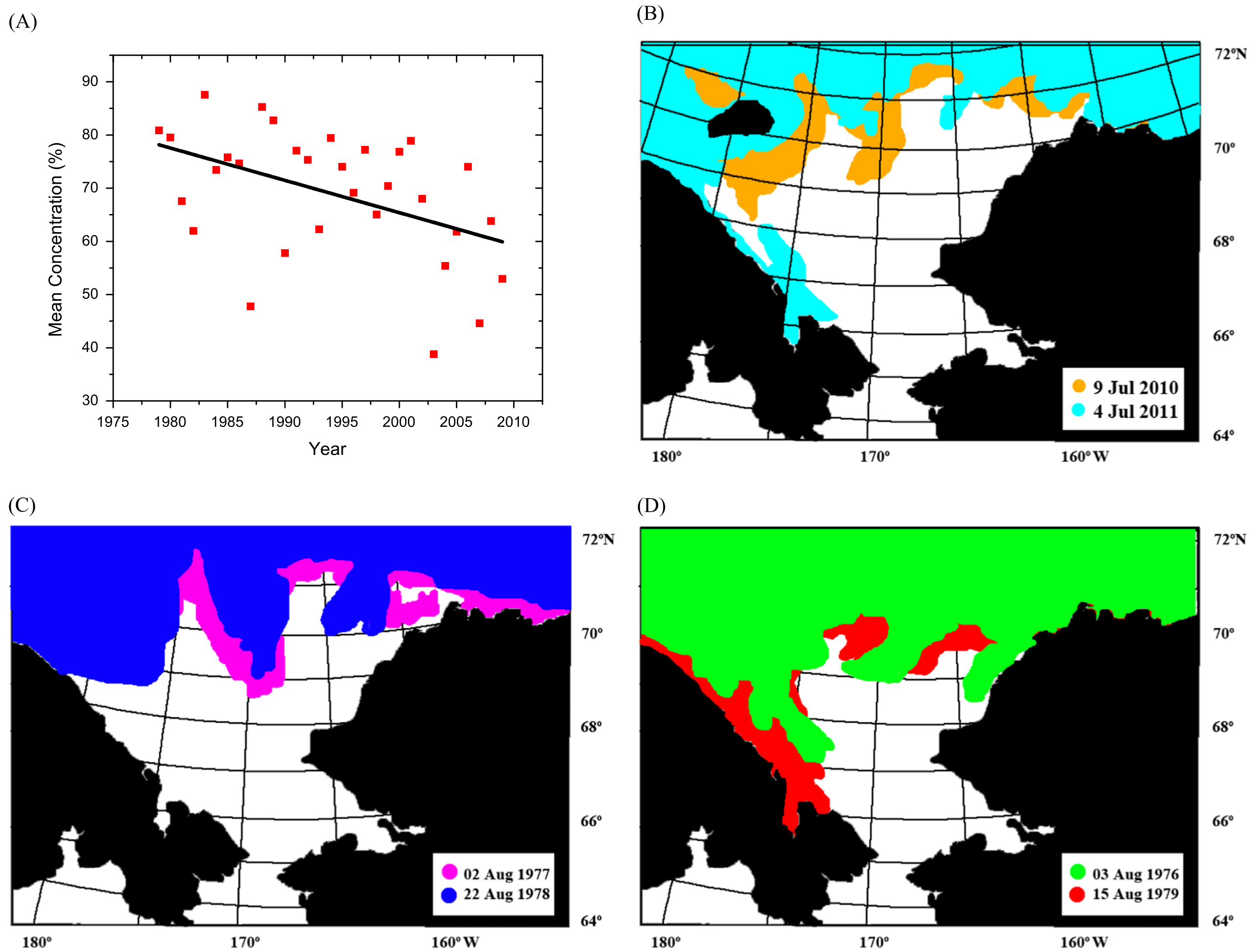

Fig. 2. (a) Mean sea ice concentration at all ICESCAPE sites during June 25–30 over the satellite era, from SMMR/SSMI NASA Team Algorithm [NSIDC, Cavalieri, et al., 1996). (b) Ice edge during ICESCAPE Missions on dates that most closely match the shape and character of the August ice edge maps presented by Paquette and Bourke (1981). (c) and (d) Ice extent from ship and aerial observations during the 1970s, from Paquette and Bourke (1981).

the region with respect to sea ice. A notable exception occurred during the 2010 mission when heavily deformed first-year ice was encountered that greatly slowed progress and caused the ship to alter course from June 24 to 27 near stations 33–36. Relative trends in ice concentration, pond coverage, and ice type seen along the way are nevertheless highly relevant to understanding ongoing changes in Chukchi – Beaufort ice cover observed during the ICESCAPE missions.

The core of the in-transit observations were conducted by observers working from the bridge of the ship to classify and report ice conditions every 2 h while the ship was in transit (Fig. 3). The Antarctic Sea ice Processes and Climate (ASPeCt) protocol (Worby et al., 1999) was used to standardize reporting, following training of all observers. Less experienced observers were paired with expert observers until consistent ice cover identification and areal extent estimation were verified. Ice thickness, concentration, and type were recorded for the primary, secondary, and tertiary ice types encountered during each watch period. First year ice was delineated from multiyear ice primarily on the basis of surface topography, but also from ice thickness. Fractional areas of melt ponds, sediment-laden ice, and biologically-rich ice were estimated visually by each observer, using reference photos as a guide to help control observations. Visibility was recorded and photographs were taken of current ice conditions. Basic meteorological observations such as air temperature, wind speed, barometric pressure, and insolation were recorded from the ship's automated meteorological systems or log observations. These observational data are archived in the NASA SeaBASS (SeaWiFS Bio-optical Archive and Storage System) archives http://seabass.gsfc.nasa.gov/.

2.3. Ice based observations

Detailed observations were also collected at 21 ice stations during the cruises – 12 in 2010 and 9 in 2011 (Table 1) (Fig. 4). Floes representative of level first year ice conditions at each location were selected for the on-ice measurements. If present, deformed first-year ice or multiyear attached to the floe was surveyed separately. During these on-ice surveys, ice thickness, pond depth, and surface scattering layer thickness were measured. Ice thickness was measured by a Geonics EM-31 electromagnetic induction sensor (Haas et al., 1997; Eicken et al.,2001; Haas and Eicken, 2001; Haas, 2004) during horizontal transects that were hundreds of meters to kilometers long, with data collected every 5 m. The geometry of transects varied from floe to floe (from a single long line to a series of parallel or intersecting lines), and was designed to effectively sample a representative mean ice thickness and (in 2011 only) melt pond depth. Sampling along transects avoided all melt ponds during 2010 for operational reasons, while ponds were sampled as encountered along by straight line transects during 2011. As a result 2010 thickness observations represent the distribution of un-ponded ice only, while 2011 observations represent a sample of all ice types in the floe.

An electromagnetic induction sensor was used for the ice thickness survey measurements and a ski pole demarked with a

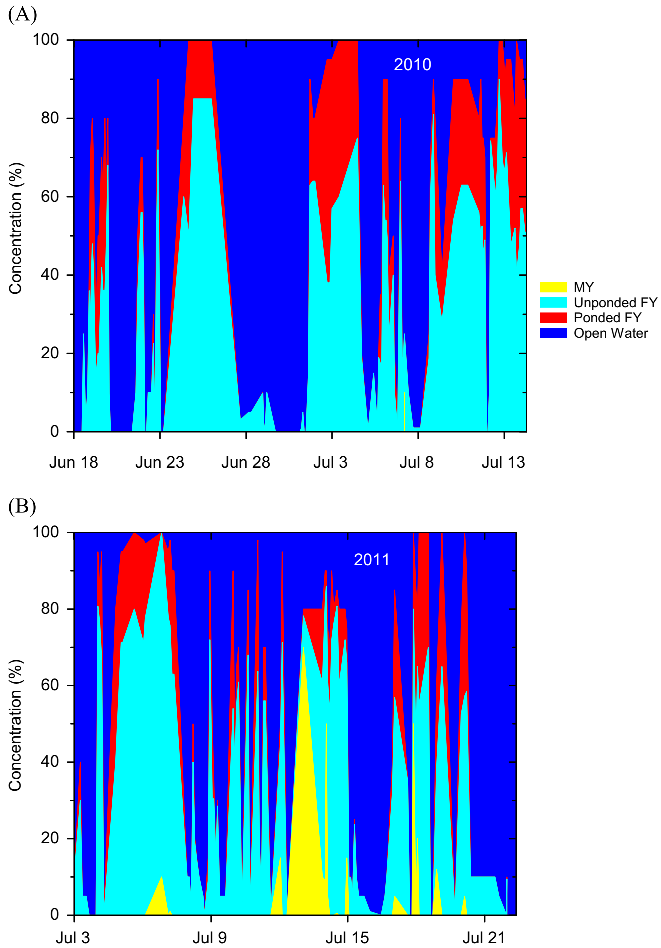

Fig. 3. Ice watch results showing the observed relative fractions of first year (FY) ice, multiyear (MY) ice, and ponded ice in 2010 and 2011 as observed from the bridge.

cm-graduated tape was used to observe pond depth and surface scattering layer thickness (Fig. 5). The EM-31 electromagnetic induction sensor determines ice thickness by exploiting the large conductivity difference between sea ice and the underlying seawater, transmitting a primary electromagnetic field and measuring the strength of the secondary field (BH1) induced in underlying seawater. The strength of the secondary field is inversely proportional to the average ice thickness over an area approximately 1.4 times the ice thickness. The EM-31 instrument is limited to a maximum sea ice thickness of 6 m and a vertical resolution of a few centimeters. Thickness surveys were conducted at 19 ice stations during the two cruises. The conversion from EM-31 response to ice thickness is dependent on the conductivity of the ice, which is influenced by salinity and brine content. All EM-31 sensor derived ice thicknesses were calculated using the transfer function (Eicken et al., 2001):

$$\text{Thickness (cm)} = 6.4019 - \frac{\ln(BH1 - 36.073)}{1.2132} * 100$$

$$- \text{antenna height above ice surface}$$

At most sites, holes were also drilled through the ice for direct measurements of ice thickness and for evaluating the coefficients in the EM-31 transfer function (Figs. 6 and 7). These measurements indicated that the transfer function used was accurate in determining sea ice thickness to within 5 cm at all sites tested, so changes in calibration coefficients from site to site were not warranted.

Ice cores were taken at each station for analyses of internal ice properties. Temperature profiles in the ice were determined by drilling 3 mm diameter holes radially into the center of the cores at 10 cm vertical intervals immediately upon extraction, and measuring temperature under shaded conditions. Salinity and oxygen isotopic composition were determined by sectioning a second core into 0.1 m vertical intervals immediately upon extraction (to minimize brine loss) and melting the sections for measurement of salinity onboard the ship using an YSI model 30 salinometer (measurement error the larger of < 0.02 or $< 1\%$ bulk salinity). Water samples for oxygen isotopic analysis ($\delta H_2^{18}O$)were collected in 20 mL glass scintillation vials, sealed with Polyseal caps and wrapped with Parafilm as a precaution to prevent evaporation and isotopic fractionation. Samples were returned to the Chesapeake Biological Laboratory of the University of Maryland Center for Environmental Science. Water samples were analyzed by equilibration with carbon dioxide using a Thermo Fisher Gas Bench II peripheral linked to a continuous flow Delta V Plus isotope ratio mass spectrometer. Results were expressed as $\delta^{18}O$ values, using the relation: $\delta^{18}O_{V\text{-}SMOW} = (R_{sample} - R_{standard}/R_{standard}) * 1000‰$, where $R = {}^{18}O/{}^{16}O$ and V-SMOW is Vienna Standard Mean Ocean Water, as distributed by the International Atomic Energy Agency. Analytical precision was better than $\pm 0.1‰$ and was assessed by analysis of in-house water standards during sample analysis and calibration to international water isotope standards (V-SMOW, V-SLAP, GISP). Data corrections were made based upon analysis of the in-house standards relative to international standards, which were normalized as per recommendations of Paul et al. (2007).

Additional 0.1 m diameter ice cores were returned intact to the Cold Regions Research and Engineering Laboratory (CRREL) for processing, where they were sliced in 0.05–0.10 m long sections to determine vertical profiles of crystallographic structure. The ice crystal structure was described by making vertical thin sections from the ice cores and then photographing these sections in both transmitted natural light and between crossed polarizers. These photographs were used to classify the ice crystallography as granular, columnar, or inclined columnar on the basis of the ice grain size and orientation (Tucker et al., 1987) in order to better understand the formation history of the ice.

3. Results and discussion

Sea ice encountered throughout the cruise was snow free, covered with numerous melt ponds, and rapidly decaying. Surface melt occurred most days, although pond surfaces regularly froze over with thin layers of ice during hours of lowest sun angle. Ongoing decay of the ice during the cruise was apparent and many areas that had ice on our northbound route were ice free on our return southward. With nearly a month of melt remaining in the summer season at the end of each cruise, it is likely that the ice we encountered melted completely before the end of summer 2010 and 2011 Regional Conditions in Context.

Ice conditions in the Chukchi and western Beaufort seas during June show considerable interannual variability in the historical record. Prevailing easterly winds typically push ice offshore, opening a substantial shore lead along the northeastern Chukchi coast in late spring well prior to the onset of melting conditions (Tremblay and Mysak, 1998). The opening of the shore lead is highly wind dependent. In some years this shore lead can be hundreds of kilometers wide by the time that melt begins in early June, whereas other years show only intermittent 10–20 km openings. Additionally, in recent years, the advection of multiyear ice into the region from the Beaufort Gyre has been irregular owing to large-scale summer melt of ice upstream in the Canadian

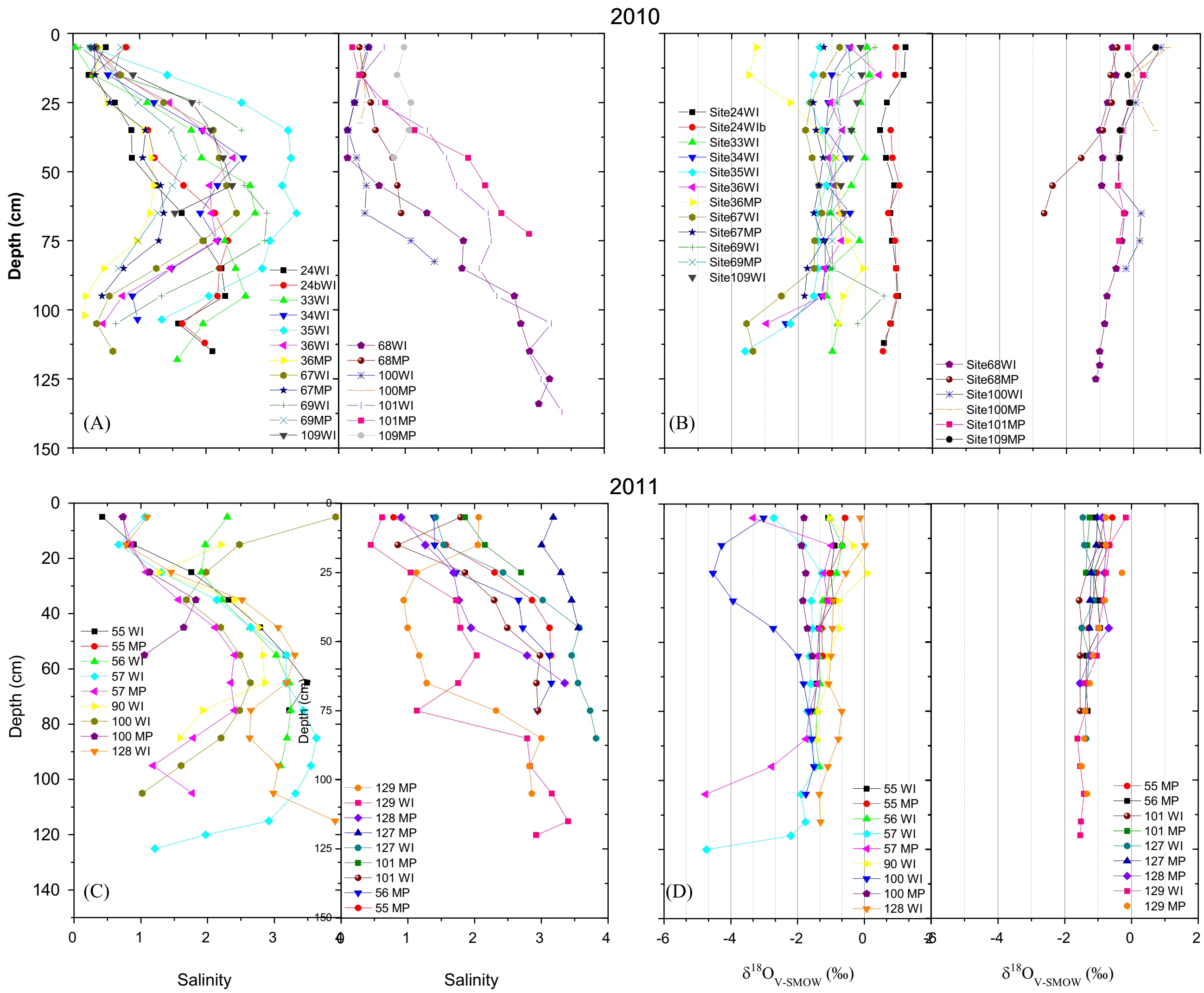

Fig. 4. Vertical profiles of salinity and $\delta^{18}O_{V\text{-}SMOW}$ from the ice stations conducted during the 2010 and 2011. Ice cores were sampled from bare white ice (WI) and melt ponded (MP) ice. Precision of the $\delta^{18}O_{V\text{-}SMOW}$ (‰) values is $\pm$0.1‰.

Table 1
Ice station dates and locations.

Station #	Date	Latitude	Longitude
2010			
9	20-Jun-10	66.74017	−163.717
24	22-Jun-10	68.30317	−166.981
33	24-Jun-10	72.03033	−159.877
34	26-Jun-10	72.11483	−160.538
35	25-Jun-10	72.0905	−160.814
36	27-Jun-10	72.06067	−161.199
67	2-Jul-10	71.69217	−159.04
68	3-Jul-10	72.1185	−157.026
69	4-Jul-10	71.64517	−157.755
100	9-Jul-10	71.73217	−156.007
101	10-Jul-10	72.0615	−156.281
109	11-Jul-10	71.93417	−156.428
2011			
55	4-Jul-11	72.63233	−168.725
56	5-Jul-11	73.165	−168.486
57	6-Jul-11	73.717	−168.264
90	10-Jul-11	72.95767	−160.766
100	12-Jul-11	73.697	−160.281
101	13-Jul-11	73.834	−159.074
127	17-Jul-11	72.54533	−153.818
128	18-Jul-11	72.83517	−151.892
129	19-Jul-11	73.1825	−150.445

Beaufort. These factors strongly influenced the ice conditions encountered during the two field programs. During 2010, strong offshore winds beginning in April created a significant amount of open water prior to the onset of melt and ice was nearly absent from the eastern half of the Chukchi Sea south of 71°N latitude and East of 166°W longitude, but present in a highly consolidated pack in the Western Chukchi during the beginning of the cruise in mid-June. During 2011, the shore lead system did not open as dramatically during spring, less open water was present prior to melt, and some multiyear ice was advected into the region. By late May, 2011 it appeared that there would be lower ice loss than in 2010 due to the significantly smaller extent of dynamically opened water. Once melt began in early June, however, the less consolidated 2011 pack retreated more quickly so that ice extent was comparatively lower for a given date by a modest margin beginning early in June. This was particularly true in the western Chukchi where wind in 2010 had produced a highly consolidated pack. In historical context, however, both years had anomalously large amounts of open water for the month of June (see 1981–2010 median ice extent line in Fig. 1) and low amounts of multiyear ice. These conditions are consistent with the recent changes observed throughout the Chukchi and Beaufort seas using passive microwave remote sensing (Comiso, 2012; Frey et al., 2014). A strong trend toward loss of ice cover can be found even in the areas

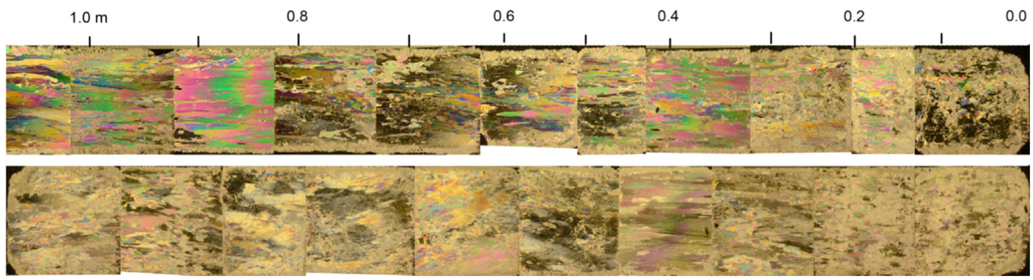

Fig. 5. Vertical profiles of ice crystallography determined from ice cores at two stations. The depth is denoted at the top of the core, the top of the core is at right. The top core shows the ice crystallography typically observed: a surface layer of granular ice with columnar ice below. The lower core shows a mix of granular, columnar, and inclined columnar, likely indicating dynamic activity during growth.

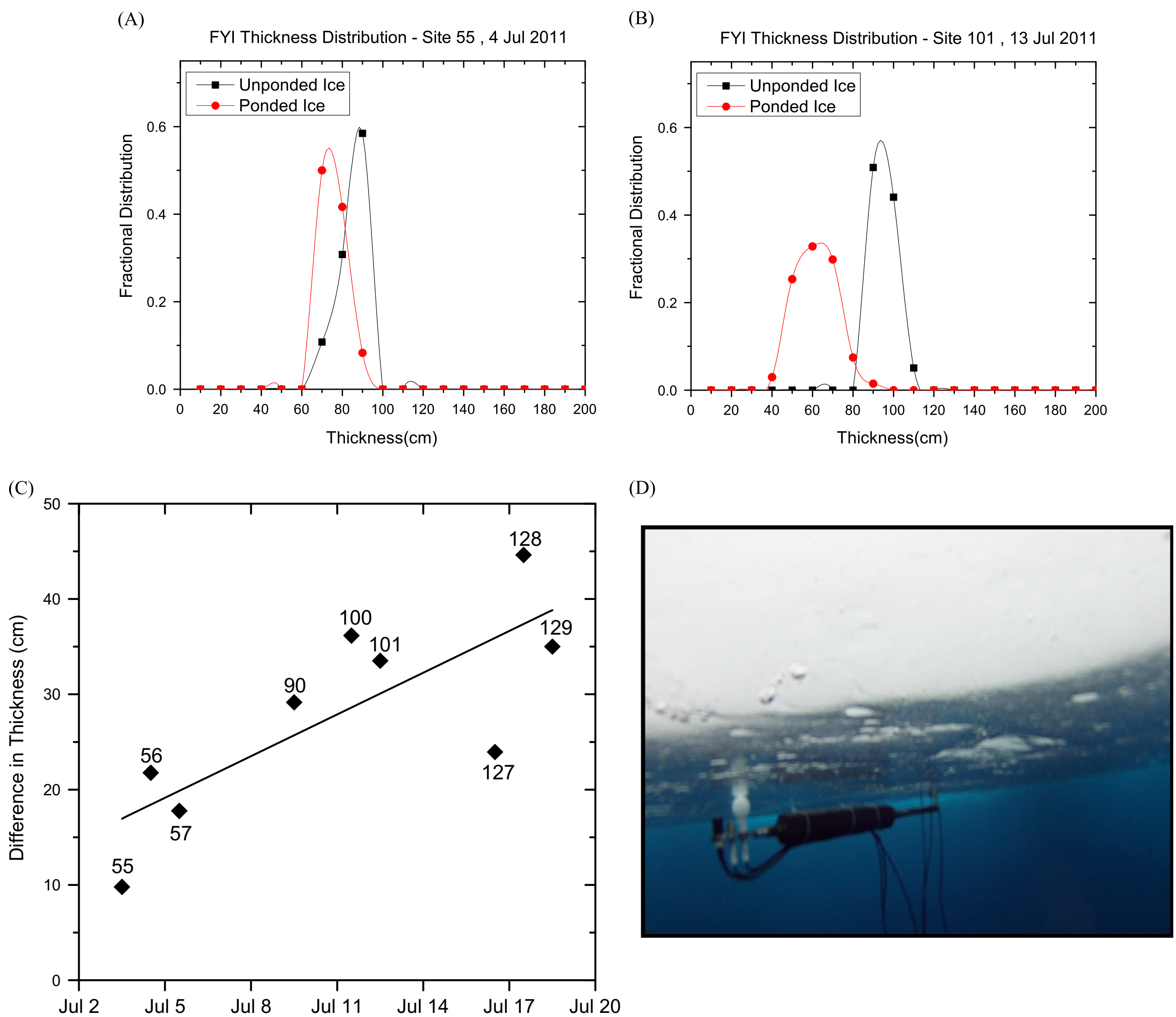

Fig. 6. Thickness distribution of ponded and unponded ice at (a) station 55 and (b) station 101, note the increasing separation between the peaks caused by faster ablation of ponded ice; (c) plot of mean unponded thickness – mean ponded thickness versus time at 2011 ice stations; (d) underice photograph showing flat bottom under undeformed ponded and unponded ice.

where ice was present during the cruise over the 1979–2009 satellite record. Average ice concentration at the locations of the 21 ICESCAPE sites (Fig. 2), calculated as an average of the daily pixel values that contain site locations over the interval June 25–30 using SMMR/SSMI NASA Team Algorithm concentration [National Snow and Ice Data Center (NSIDC), Cavalieri et al., 1996) shows a decline of approximately 20% concentration over the 30-year timeframe.

In addition to remote sensing observations avialable since the late 1970s, a number of research cruises in the Chukchi – Beaufort region that made observations of ice morphology and physical properties have been conducted in the past. These observations (including those collected by the five MIZPAC (Marginal Sea Ice Zone Pacific) expeditions (1971–1977), Arctic Summer West Experiment (1992), 1997–1998 SHEBA (Surface Heat Budget of the Arctic Ocean) deployment and retrieval transits, the

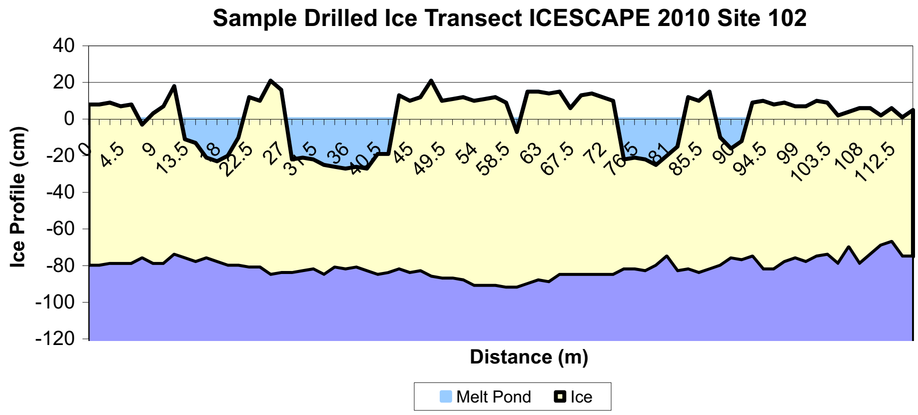

Fig. 7. Ice thickness, freeboard, and melt pond depth measured along a 120 m transect on undeformed first year ice.

2002–2005 SBI (Shelf-Basin Interactions) project, and the 2005 HOTRAX ((Healy-Oden Trans Arctic Expedition) transit) all provide a basis for comparison. The MIZPAC expeditions, which extend our records back prior to the satellite era are of particular interest. In summarizing the ice encountered during those expeditions, Paquette and Bourke (1981) wrote, "The southern portion of the Chukchi Sea is ice covered for nearly 8 months of the year, and the ice remains south of 71 °N for 10 or 11 months. The ice begins to disappear at the Bering Strait in about late June, after which melting is rapid under the influence principally of the warm 6–10 °C northward flowing water. The ice reaches maximum retreat at approximately 72–75 °N in mid-September." The pattern of retreat observed during the MIZPAC experiment is similar to that observed in 2010 and 2011, but the timing of breakup and position of the ice edge at its summer minimum have substantially changed. In particular, the ice extent for early July 2010 and 2011 can be compared to ice extent observed from ship and aircraft records from August 1977–1978 (Fig. 2). Although the general position of the ice edge in 2010–2011 during retreat was roughly a month earlier than during the MIZPAC experiments of the 1970s, similar patterns of retreat were observed, suggesting that the mechanisms of heat delivery and ice movement active in the 1970s are still at play. Indentations are observed along the ice edge with faster sea ice retreat, and are aligned with sea floor troughs with higher northward current flow while sea ice extends further south ('peninsulas' of sea ice) over shallow shoals (e.g. Herald and Hanna Shoals). These patterns indicate that the ice edge location is likely governed by a combination of ocean currents delivering heat from open water and ultimately North Pacific sources, as well as ice grounding on the shallow shoals (Martin and Drucker, 1997; Weingartner et al., 2005; Woodgate et al., 2006). During recent years, however, this system of indentations into the sea ice edge has not endured into late summer as during the MIZPAC observations. Instead, the end of summer ice edge in the Chukchi Sea has continued to retreat northward and has been well north of 75 °N latitude in the past several years by late summer. This is expected both from the lack of bathymetric current steering beyond the shelf break, and the potential for the influence of advected heat from the Pacific to increasingly give way to locally absorbed solar energy.

3.1. ASPeCt in transit observations

Observations of ice type, pond coverage, ice deformation, and sediment content were made from the bridge of the ship while underway using the ASPeCt protocol (Fig. 3). Consistent with remote sensing observations, the Eastern (U.S.) side of the Chukchi Sea, which historically contained first year ice during late June and early July Paquette and Bourke (1981), was largely ice-free during June 2010 and 2011. Additionally, the northern extremes of the Chukchi continental shelf (north of 70°N), historically contained predominantly multiyear ice Paquette and Bourke (1981), but contained mostly first year ice during these observations, with only isolated areas and low concentrations of multiyear ice. The observed ice concentrations therefore, indicated a significant shift in both the makeup of the pack and the timing of its retreat.

Table 2
Mean ice thickness from 2010 ICESCAPE mission (where all stations were on first year (FY) ice).

Date	Station	Ice type	Unponded ice thickness (cm)
6/24/2010	33	FY Undeformed	116
6/25/2010	34	FY, Some Deformed	163
6/26/2010	35	FY, Some Deformed	152
7/1/2010	36	FY Deformed	201 (*excludes some > 6 m)
7/2/2010	67	FY, Some deformed	138
7/3/2010	68	FY Undeformed	110
7/8/2010	69	FY Undeformed	120
7/10/2010	101	FY Undeformed	109

Melt ponds were ubiquitous on the ice during both ICESCAPE missions, ranging from less than 5% coverage on heavily deformed ice to 65% coverage on thin undeformed first year ice in late stages of melt. Overall, mean pond coverage was more prevalent in 2010 (29% of ice coverage) than in 2011 (19% of ice coverage). The variation observed was likely due to a higher prevalence of multiyear ice (which has lower pond coverage) and thicker first year ice coverage in 2011. A strong relationship was noted between pond coverage and ice thickness, with greater coverage occurring as the ice thinned and lost the buoyancy required to keep large areal fractions of the surface above freeboard. We arrived 2–4 weeks after the onset of melt in the study area and, based on high water marks on the floes, melt ponds appeared to already have passed through an above-sea-level surface flooding stage with much greater melt pond coverage and then drained to sea level shortly before our arrival. Many drainage features were present, indicating that significant pond drainage occurred via over-ice flow to flaws and cracks, consistent with observations of Polashenski et al. (2012).

Sediment contained in the ice, entrained during the freezing process, has a significant impact on ice albedo and transmission of light through the ice. Ice entrained sediments were visible on floes throughout the region in both years (40% of shipboard observations in 2010 and 35% in 2011). The sediment loading varied from light and barely perceptible to a few cases of solid layers of mineral matter several centimeters thick atop isolated floes. The prevalence of sediment rich ice was typically well below 100%. The

Table 3
Mean ice thickness from 2011 ICESCAPE mission (where stations were on both first year (FY) and multiyear (MY) ice).

Date	Station	Ice type	All ice	Thickness (cm)		Pond depth
				Unponded Ice	Ponded ice	
7/4/2011	55	FY Undeformed	76	80	70	5
7/5/2011	56	FY Undeformed	103	110	88	11
7/6/2011	57	FY Undeformed	120	125	107	12
7/6/2011		FY Deformed/MY	230	239	199	28
7/10/2011	90	FY Deformed	176	198	110	23
7/10/2011		FY Undeformed	86	92	63	26
7/12/2011	100	Young MY	173	189	131	31
7/12/2011		Young MY Hummock	300	300	None	None
7/12/2011		FY Undeformed	98	116	80	25
7/12/2011		Old MY	> 600	N/A	N/A	N/A
7/13/2011	101	FY Undeformed	73	91	57	27
7/13/2011		FY Deformed/MY	133	140	99	22
7/17/2011	127	FY Undeformed	84	91	67	18
7/17/2011		MY	155	166	96	18
7/18/2011	128	FY Undeformed	101	120	75	25
7/18/2011		MY	202	197	208	22
7/19/2011	129	FY Undeformed	101	117	82	23
7/19/2011		FY Deformed	137	156	93	23

weighted incidence of sediment-entrained ice by area for all observations was 7.5% in 2010 and 10.9% in 2011.

3.2. *Internal ice properties – temperature, salinity, $\delta^{18}O$ values, and crystallography*

Temperatures within ice cores were close to isothermal, varying only from 0 to −1 °C. Typical temperatures were near 0 °C at the top and bottom of the ice profiles with slightly colder temperatures in the middle of the core where brine concentrations remain higher. The warm ice bottom (near 0 °C) is a clear indication that stratified fresh water from ice and snowmelt and drainage off the ice surface was in contact with the ice bottom. The presence of freshwater lenses beneath the ice was observed at many sites, particularly in 2010. Only a few cases of colder ice at the bottoms of cores were found, indicating ice bottom contact with more saline ocean waters.

The majority of the salinity profiles (Fig. 4a and c, left panel) had very low salinity in the uppermost and lowermost parts of the core (<2.5) and maximum salinity (1.5–4) within the colder interior ice. These salinities represent a mirror image of the characteristic 'C' shaped profiles observed in cold, growing first year sea ice where high salinity is observed in the uppermost ice (where growth was fastest and most likely granular) and lowermost ice (where brine rejection is not yet complete). The maximum salinities observed are also well below the range typically observed in cold, first year sea ice [4–9; Weeks and Ackley, 1982). These results indicate that the ice had reached an advanced state of melt prior to our sampling and that brine loss was well underway. The shape of the profiles indicates that two previously identified mechanisms of brine rejection were active prior to the observations; (1) meltwater flushing brine from the upper ice and (2) convective replacement of brine in the lower ice with fresher water from below (Eicken et al., 2002: Notz and Worster, 2009). The conditions necessary to support both of these processes were present. Rapid melt was underway for at least 2 weeks prior to our sampling, indicating that an ample supply of surface freshwater had been present for flushing. Freshwater lenses were regularly observed immediately beneath the ice, confirming the presence of low-density fresh water beneath the ice needed to support convective brine replacement in the lower ice.

A second type of salinity profile exhibited increasing salinity with depth and highest salinities in the lowermost part of the ice (Fig. 4a and c right panel). These frequently observed sites likely had weaker or non-existent convective brine overturning desalinating the bottom of the ice. Sites with these profiles all lacked stratified freshwater beneath the ice in the area of the coring, indicating that weaker convective brine replacement in the lower ice had allowed higher brine concentrations to remain within the ice. We had expected that this second profile type would be less common during active melt owing to additional opportunities for overturning. However, the two profile types were evenly distributed regardless of date during each year's observations. Comparing the two years, the 2011 cruise (starting 2 weeks later than in 2010) exhibited more profiles of the second profile category, which is consistent with observations of fewer under ice freshwater lenses in 2011. For both profile types, cores taken in ponded ice exhibited lower average and peak salinity. Visually inspecting the cores revealed that internal melt in ponded ice was much more advanced than in unponded ice, a likely result of lower albedo and enhanced solar absorption in the darker ponds. The advanced internal melt made brine pockets more connective, and combined with presence of greater amounts of meltwater for flushing allowed for greater desalination via freshwater flushing.

$\delta^{18}O$ values (Fig. 4b and d) of the ice were clustered in a relatively narrow range of 0 to −2.5‰, and in most cases, with the largest changes in isotopic composition towards more negative values at the bottom of cores. Principal factors impacting $\delta^{18}O$ values in sea ice include the $\delta^{18}O$ value of the parent water mass from which ice grew and the growth rate of the ice (Toyota et al., 2013). Ice has a higher $\delta^{18}O$ value than the parent water which it formed due to preferential fractionation of the heavier ^{18}O-bearing isotopomer of water ($H_2^{18}O$) into the sea ice during freezing and the degree of fractionation is also dependent on the freezing rate (Toyota et al., 2013; O'Neill, 1968). Under growth conditions typical for sea ice, the fractionation varies from $<0.1^0/_{00}$ for fast growing frazil ice to $>2.5^0/_{00}$ for slow growing columnar ice (Souchez et al., 2000; Souchez et al., 1987; Eicken, 1998; Smith et al., 2012; Toyota et al., 2013), with a range of $1.5-2.5^0/_{00}$ capturing the fractionation corresponding to the growth rates of most natural sea ice. Typical summer $\delta^{18}O$ values in surface waters of the Arctic Basin range from −4‰ for areas subject to large river runoff such as the southeastern Beaufort (Mackenzie River) and the Laptev, Kara, and East Siberian Seas (Lena, Ob, Yenisei Rivers) to −2‰ for Central Arctic Basin waters and +1‰ for Atlantic-influenced Barents sea waters. Within the probable formation areas of ice encountered in the Chukchi Sea, parent summer water masses can range from −4‰ 'upstream' in the Beaufort Gyre to −1‰ on the Chukchi Shelf itself (Pfirman et al., 2004; NASA Global O18 database – http://data.giss.nasa.gov/o18data/).

Given fractionation of around $+2^0/_{00}$ and expected parent masses of −4‰ to −1‰, the bulk of our samples lie in the expected range. The general trend toward more negative $\delta^{18}O$

values at greater depths in many core observations (Fig. 4b and d), however, is opposite to what would be expected from typical changes in ice growth. Generally, growth rates of sea ice decrease as the sea ice gets thicker due to the longer pathway (through the thickening ice) by which heat from additional freezing must be removed. The slower freezing rate results in a larger isotopic fractionation (relatively more positive $\delta^{18}O$ values in ice that formed more slowly). The observations to the opposite of these expectations suggest that water mass changes play a larger role than isotopic fractionation during freezing.

Therefore it is possible that the general pattern of more negative $\delta^{18}O$ values at the bottom of cores reflect sea ice passing over surface waters with a relatively strong meteoric signal at the end of the sea ice formation season. The observations of increasingly negative $\delta^{18}O$ values, particularly at the base of the sea ice, suggest passage of the ice under freezing conditions over surface waters with a significant runoff signal, along with perhaps fast sea ice formation. Brine injection events over the winter mix surface waters and dilute the meteoric water signal as ice moves southwest onto the Chukchi Shelf from deeper waters in the Beaufort Sea. For example, surface waters sampled in May 2002 under subfreezing conditions, during a SBI project cruise in Hanna Valley, ranged from -1.0 to -1.2‰, consistent with northward flowing Bering Sea winter water (Cooper et al., 2005; Cooper et al., 2006). During the same cruise, surface waters over deeper portions of Barrow Canyon showed a much stronger meteoric signal (-2 to -3‰; Cooper et al., 2005). A similar pattern is observed for ICESCAPE stations located in the most eastward and northerly sectors of the study area (unpublished data). For example, surface waters at Station 99 on the 2011 cruise (73.539°N, 159.918°W) were observed to have $\delta^{18}O$ values of <-3, while $\delta^{18}O$ values on the Chukchi shelf were closer to ~-1.5‰, which is consistent with the prior SBI project observations. The ice core patterns observed with more negative $\delta^{18}O$ values at the bottom of cores suggest active ice formation while the growing ice passed over waters of the Beaufort Sea where there is a stronger runoff influence. However, by the time the sea ice was advected onto the Chukchi Shelf, sea ice growth had slowed or stopped, and therefore the less negative $\delta^{18}O$ values present in surface water (made up largely of Bering Sea winter water) was not incorporated significantly into the bottom of the sea ice.

Thus, the observations of increasingly negative $\delta^{18}O$ values with sea ice depth could be explained under a scenario where sea ice thickness grew under late winter conditions as the sea ice passed over deeper Beaufort Sea waters with high river runoff content and sea ice formation had stopped by the time these cores were collected, primarily over shelf waters. This implies also that initial sea ice formation occurred in waters with relatively low meteoric runoff.

Another possibility is that meteoric water provided by snowmelt could have percolated into the ice. The meteoric water originating from snowmelt could potentially obscure patterns in the ice that record surface water or growth history (e.g. Pfirman et al., 2004). Increased concentrations of meteoric water entrained in the deeper ice by freshwater refreezing during brine flushing might create the pattern we observe. Entrainment of meteoric water into the ice is likely (as we discuss below), however we lack a clear explanation for such a regular, gradual trend in meteoric water entrainment with depth, leaving change in parent water mass more likely.

Superimposed on the general trend of lower $\delta^{18}O$ values at depth are several more dramatic negative deviations in $\delta^{18}O$ in the top and bottom layers of the cores that can be attributed to meteoric water entrainment. The magnitude of these variations is greater than the expected variation in surface ocean water from this region. Though it is possible that these low $\delta^{18}O$ values indicate that the ice formed from near shore, river discharge-influenced water mass, it is more likely they indicate that meteoric water of low $\delta^{18}O$ value from snowmelt was entrained into the ice. In the lower ice pack, this occurs by convective brine replacement from meltwater lenses beneath the ice. We know that meltwater lenses were present due to widespread observations of false bottoms, a layer of ice which forms at the interface of an under-ice freshwater lens and the colder, more saline ocean water. (Notz et al., 2003; Perovich et al., 2003) False bottoms were present at nearly all sites in 2010, but are challenging to collect in the core barrel. These core samples, therefore, do not include distinct layers of false bottom ice that were present. Additional cases where low $\delta^{18}O$ was observed in the uppermost layers of the ice are likely due to the presence of melted snow that refroze. On the ice surface this is likely due to the formation of superimposed ice from snowmelt refreezing in a discrete layer, while within the ice column, isotope depleted water may have been emplaced as percolating meltwater re-froze in brine channels and pockets when fresh intruding meltwater initially encountered cold ice (Polashenski et al., 2012). Site 100, collected in 2011, shows a particularly low $\delta^{18}O$ values within the interior of the ice core. This was likely caused by ice rafting that entrained snow within the ice earlier in the year. This interpretation is supported by the anomalous salinity profile likewise observed at this site.

Two profiles collected during the 2010 mission at site 24, the southern Chukchi Sea (Fig. 4b), show $\delta^{18}O$ values above 0 throughout the core profile. We do not have a satisfactory explanation for why these samples are enriched in $\delta^{18}O$, although sequential partial thaw and re-freezing of sea ice could possibly increase the residual isotopic content of heavier isotopes of water. Simply based upon the isotopic content of freezing surface waters, all water in the study area should produce ice of near zero or lower $\delta^{18}O$ values.

Thin sections made from the ice cores showed that there was variability in ice structure vertically within cores and from core to core. Typically the top 0.1 m of the ice was granular, with columnar ice below. Occasionally however, there were layers of granular ice within the ice interior. In general, ice cores were 70–80% columnar, with the remainder granular or a mix of granular and columnar (see Fig. 5 for two representative ice stations).

3.3. Ice thickness

The mean thickness values presented here (Tables 2 and 3) are based on a representative sample of the ice thickness in each type, consisting of 100–400 thickness observations. The predominant ice type, undeformed first year ice, varied in mean thickness from 0.73 to 1.2 m (Tables 2 and 3). Floe measurements excluded ice thinner than about 0.75 m, which was often present in the area.

By midsummer, the impact of maximum ice growth during the prior winter and melt rates during the current summer on the observed ice thickness are fully convolved and the relative impact of each process is challenging to interpret. One area where the impact of melt appeared to dominate was on the S–N transect from sites 55–57 in 2011, where ice thickness increased from 76 cm to 120 cm across three sites as the ship moved further into the ice pack. These increasing ice thicknesses with distance into the pack were consistent with the shipboard measurement trend in ice thickness observed in transit. We conclude that this thickness gradient was likely caused by warmer waters transported northward underneath the ice delivering heat to the underside of the ice and causing it to melt. We considered and rejected alternate hypotheses which could have created this gradient in thickness, such as a gradient in surface melt rates or a gradient in the ice thickness prior to the onset of melt caused by differing winter growth. Melt ponds along the transect from station 55–57 were of very similar maturity and the difference in thickness between ponded and unponded ice actually increased slightly as we progressed northward (see next paragraph), indicating that the northern ice (which we encountered 1 and 2 days later in time) was actually at a slightly more advanced state of melt. Similarly, the thickness of the largest up-heaved ice blocks contained in ridge formations, recorded by the ASPeCt observers along the route were consistent, suggesting that the ice grew to similar thickness at the end of winter. The ultimate heat source being transported northward under the ice was likely a combination of energy carried north from the Pacific in currents through Bering Strait and local solar absorption in the Chukchi Sea. Although our data are not sufficient to determine the fraction of heat coming from each heat source, the initial heat influx was most likely dominated by Pacific water, while the opportunity for local solar heating and the role of energy absorbed in open water most likely grew with increasing open water area, as expected in a classic ice-albedo feedback scenario.

The albedo feedback impact of added solar absorption in melt ponds is also readily apparent from the thickness measurements (Fig. 6a and b). Undeformed first year ice tends to be very uniform in thickness prior to the onset of melt (Sturm et al., 2006), with snow-free areas that later become melt ponds actually slightly thicker owing to enhanced thermal loss in these areas during winter. Here however, we see that the ponded and unponded ice thickness distribution peaks were already well separated by the time we sampled after July 3, 2011 (with ponded ice much thinner). The difference in ice thickness between ponded and unponded ice accelerated by 1.5 cm per day ($r^2=0.56$) as more rapid melting in the ponds preferentially thinned ponded ice by July 13 (e.g. Fig. 6c). Drilled profiles (Fig. 7) and underwater photography (Fig. 6d) indicate that the ice bottom was nearly horizontal in regions of undeformed ice, even near the end of the sampling, so the difference in thickness between ponded and unponded ice was almost entirely attributable to differential surface melt.

4. Conclusions

A significant shift in the makeup of the ice pack and the timing of ice retreat has occurred in the Chukchi and western Beaufort seas over the past several decades. Observations collected during the 2010 and 2011 NASA ICESCAPE missions confirm that ice retreat occurred during these two years substantially earlier than in the historic record, and that the overall makeup of the pack has shifted toward younger, thinner ice. Evidence of enhanced bottom melting near the ice edge in the central Chukchi Sea confirm that heat transport in bathymetrically steered currents played an important role in the geometry of the ice retreat. Characteristics of the ice, particularly the large pond fraction and low multiyear ice fraction suggest that the upper ocean of the Chukchi sea is likely receiving more transmitted light than it did in past decades. The regime shift in the physical properties and morphology of ice has substantial implications for thermodynamic forcing, light availability in the upper ocean, and biological and biogeochemical processes in the ice and water column beneath.

Acknowledgments

This research was supported by the NASA Impacts of Climate change on the EcoSystems and Chemistry of the Arctic Pacific Environment (ICESCAPE) project with support from the NASA Cryospheric Sciences Program (Grant #NNX10AH71G to K. Frey, L.W. Cooper, and J.M. Grebmeier and Grant #NNH10A017IE to D. Perovich and B. Light) and the NASA Ocean Biology and Biogeochemistry Program. The field component of this research would not have been possible without the tremendous support from the commanding officer, marine science technicians, crew, and officers of *USCGC* Healy on the HLY1001 and HLY 1101 missions to the Chukchi and Beaufort seas in June–July 2010 and 2011. We acknowledge and appreciate comments by two anonymous reviewers which helped to improve this manuscript.

References

Arrigo, K., Perovich, D.K., et al., 2012. Massive phytoplankton blooms under Arctic sea ice. Science, 336.
Cavalieri, D., Parkinson, C., Gloersen, P., Zwally, H.J., 1996. Sea ice concentrations from Nimbus-7 SMMR and DMSP SSMI passive microwave data. Digital media, National Snow and Ice Data Center, Boulder, Colorado, updated, 2006.
Cavalieri, D.J., Parkinson, C.L., 2012. Arctic sea ice variability and trends, 1979–2010. The Cryosphere 6, 881–889. http://dx.doi.org/10.5194/tc-6-881-2012.
Comiso, J.C., 2012. Large decadal decline of the Arctic multiyear ice cover. J. Clim. 25, 1176–1193.
Cooper, L.W., Ronald, B., James, W.M., Bruce, J.P., Robert, M.H., Peter, A.R., Dennis, A.H., Jacqueline, M.G., Louis, A.C., 2005. Linkages among runoff, dissolved organic carbon, and the stable oxygen isotope composition of seawater and other water mass indicators in the Arctic Ocean. J. Geophys. Res., 110.
Cooper, L.W., Codispoti, L.A., Kelly, V., Sheffield, G., Grebmeier, J.M., 2006. The potential for using Little Diomede Island as a platform for observing environmental conditions in Bering Strait. Arctic 59, 129–141.
Eicken, H., Tucker III, W.B., Perovich, D.K., 2001. Indirect measurements of the mass balance of summer Arctic sea ice with an electromagnetic induction device. Ann. Glac., 194–200.
Eicken, H., Krouse, H.R., Kadko, D., Perovich, D.K., 2002. Tracer studies of pathways and rates of meltwater transport through Arctic summer sea ice. J. Geophys. Res. 107 (C10), 8046. http://dx.doi.org/10.1029/2000JC000583.
Eicken, H., 1998. Factors determining microstructure, salinity and stable-isotope composition of Antarctic sea ice: deriving modes and rates of ice growth in the Weddell Sea. AGU Antarctic Research Series, 74. M.O. Jeffries (Ed.), Antarctic Sea Ice Physical Processes, Interactions and Variability, pp. 89 – 122.
Frey, K.E., Maslanik, J.A., Kinney, J.C., Maslowski, W., 2014. Recent variability in sea ice cover, age, and thickness in the Pacific Arctic Region. In: Grebmeier, J.M., Maslowski, W. (Eds.), The Pacific Arctic Region: Ecosystem Status and Trends in a Rapidly Changing Environment. Springer, pp. 31–63.
Giles, K.A., Laxon, S.W., Ridout, A.L., 2008. Circumpolar thinning of Arctic sea ice following the 2007 record ice extent minimum. Geophys. Res. Lett. 35, L22502. http://dx.doi.org/10.1029/2008GL035710.
Haas, C., Gerland, S., Eicken, H., Miller, H., 1997. Comparison of sea-ice thickness measurements under summer and winter conditions in the Arctic using a small electromagnetic induction device. Geophysics 62 (3), 749–757.
Haas, C., Eicken, H., 2001. Interannual variability of summer sea ice thickness in the Siberian and central Arctic under different atmospheric circulation regimes. J. Geophys. Res. 106, 4449–4462.
Haas, C., 2004. Late-summer sea ice thickness variability in the Arctic Transpolar Drift 1991–2001 derived from ground-based electromagnetic sounding. Geophys. Res. Lett. 31, L09402. http://dx.doi.org/10.1029/2003GL019394.
Haas, C., Hendricks, S., Eicken, H., Herber, A., 2010. Synoptic airborne thickness surveys reveal state of Arctic sea ice cover. Geophys. Res. Lett. 37, 9.
Jeffries, M., Overland, J.E., Perovich, D.K., 2013. The Arctic shifts to a new normal. Phys Tod. 66, 35–40.
Kwok, R., Rothrock, D.A., 2009. Decline in Arctic sea ice thickness from submarine and ICESat records: 1958–2008. Geophys. Res. Lett. 36 (L15501), http://dx.doi.org/10.1029/2009GL039035.
Laxon, S.W., et al., 2013. CryoSat-2 estimates of Arctic sea ice thickness and volume. Geophys. Res. Lett., 40. http://dx.doi.org/10.1002/grl50193.
Markus, T., Stroeve, J.C., Miller, J., 2009. Recent changes in Arctic sea ice melt onset, freezeup, and melt season length. J. Geophys. Res. 114, C12024. http://dx.doi.org/10.1029/2009JC005436.
Martin, S., Drucker, R., 1997. The effect of possible Taylor columns on the summer ice retreat in the Chukchi Sea. J. Geophys. Res. 102 (C5), 10473–10482.
Maslanik, J., Stroeve, J., Fowler, C., Emery, W., 2011. Distribution and trends in Arctic sea ice age through spring 2011. Geophys. Res. Lett. 38, L13502. http://dx.doi.org/10.1029/2011GL047735.
Nghiem, S.V., I.G. Rigor, D.K., Perovich, P., Clemente-Colón, J.W., Weatherly, Neumann, G., 2007. Rapid reduction of Arctic perennial sea ice. Geophys. Res. Lett. 34, L19504. http://dx.doi.org/10.1029/2007GL031138.
Notz, D., McPhee, M.G., Worster, M.G., Maykut, G.A., Schlünzen, K.H., Eicken, H., 2003. Impact of underwater-ice evolution on Arctic summer sea ice. J. Geophys. Res.: Oceans 108 (C7), 1978–2012.
Notz, D., Worster, M.G., 2009. Desalination processes of sea ice revisited. J. Geophys. Res.: Oceans 114 (C5), 1978–2012.
O'Neill, J.R., 1968. Hydrogen and oxygen isotopic fractionation between ice and water. J. Phys. Chem. 72, 3683–3684.
Paquette, R.G., Bourke, R.H., 1981. Ocean circulation and fronts as related to ice melt-back in the Chukchi Sea 1978–2012. J. Geophys. Res.: Oceans 86 (C5), 4215–4230.

Paul, D., Skrzypek, G., Fórizs, I., 2007. Normalization of measured stable isotopic compositions to isotope reference scales–a review. Rapid Commun. Mass Spectrom. 21, 3006–3014.
Perovich, D.K., Grenfell, T.C., Richter-Menge, J.A., Light, B., Tucker, W.B., Eicken, H. (2003). Thin and thinner: Sea ice mass balance measurements during SHEBA. J. Geophys. Res.: Oceans (*1978–2012*),*108*(C3).
Perovich, D.K., Richter-Menge, J.A., Jones, K.F., Light, B., 2008. Sunlight, water, and ice: Extreme Arctic sea ice melt during the summer of 2007. Geophys. Res. Lett. 35, L11501. http://dx.doi.org/10.1029/2008GL034007.
Perovich, D.K., Richter-Menge, J.A., Jones, K.F., Light, B., Elder, B.C., Polashenski, C.M., LaRoche, D., Markus, T., Lindsay, R., 2011. Arctic sea ice melt in 2008 and the role of solar heating. Ann. Glaciol. 52, 355–359.
Perovich, D.K., Polashenski, C., 2012. Albedo evolution of seasonal Arctic sea ice. Geophys. Res. Lett. 39, L08501. http://dx.doi.org/10.1029/2012GL051432.
Pfirman, S.L., Haxby, W., Eicken, H., Jeffries, M., Bauch, D., 2004. Drifting Arctic sea ice archives changes in ocean surface conditions. Geophys. Res. Lett. 31, http://dx.doi.org/10.1029/2004GL020666.
Polashenski, C., Perovich, D., Courville, Z., 2012. The mechanisms of sea ice melt pond formation and evolution. J. Geophys. Res. 117, C01001. http://dx.doi.org/10.1029/2011JC007231.
Smith, I.J., Langhorne, P.J., Frew, R.D., Vennell, R., Haskell, T.G., 2012. Sea ice growth rates near ice shelves. Cold Reg. Sci. Technol. 83–84 (0), 57–70.
Souchez, R., Tison, J.-L., Jouzel, J., 1987. Freezing rate determination by the isotopic composition of the ice. Geophys. Res. Lett. 14 (6), 599–602.
Souchez, R., Jouzel, J., Lorrain, R., Sleewaegen, S., Stiévenard, M., Verbeke, V., 2000. A kinetic isotope effect during ice formation by water freezing. Geophys. Res. Lett. 27 (13), 1923–1926.
Sturm, M., Maslanik, J., Perovich, D., Stroeve, J., Richter-Menge, J., Markus, T., Holmgren, J., Heinrichs, J., Tape, K., 2006. Snow depth and ice thickness measurements from the Beaufort and Chukchi Seas collected during the AMSR-Ice 03 Campaign. Trans. Geosci. Remote Sens. 44 (11), 3009–3020.
Toyota, T., Smith, I., Gough, A., Langhorne, P., Leonard, G., Van Hale, R., Mahoney, A., Haskell, T., 2013. Oxygen isotope fractionation during the freezing of sea water. J. Glaciol. 59 (216), http://dx.doi.org/10.3189/2013JoG12J163.
Tucker, W.B., Gow, A.J., Weeks, W.F., 1987. Physical properties of summer sea ice in the Fram Strait. J. Geophys. Res.: Oceans (1978–2012) 92 (C7), 6787–6803.
Tremblay, L.-B., Mysak, L.A., 1998. On the origin and evolution of sea-ice anomalies in the Beaufort – Chukchi Sea. Clim. Dyn. 14.6, 451–460.
Weeks, W.F., Ackley, S.F., 1982. The growth, structure, and properties of sea ice. CRREL Monograph, 82-1. Cold Regions Research and Engineering Laboratory, Hanover p. 130.
Weingartner, T., Aagaard, K., Woodgate, R., Danielson, S., Sasaki, Y., Cavalieri, D., 2005. Circulation on the north central Chukchi Sea shelf. Deep-Sea Res. Part II-Top. Stud. Oceanogr. 52 (24 – 26), 3150–3174. http://dx.doi.org/10.1016/j.dsr2.2005.10.015.
Woodgate, R.A., Aagaard, K., Weingartner, T.J., 2006. Interannual changes in the Bering Strait fluxes of volume, heat and freshwater between 1991 and 2004. Geophys. Res. Lett. 33 (15), 1–5.
Worby, Anthony P., I.a.n. Allison, and Vito Dirita (1999), A technique for making ship-based observations of Antarctic sea ice thickness and characteristics. Antarctic CRC.